Pergamon

Cement and Concrete Research 31 (2001) 1427–1436

CEMENT AND CONCRETE RESEARCH

Detection of the corrosion damage of rebar in concrete using impact-echo method

Ming-Te Liang*, Po-Jen Su

Department of Harbor and River Engineering, National Taiwan Ocean University, Number 2, Pei-Ning Road, Keelung 20224, Taiwan, ROC

Received 7 July 2000; accepted 6 June 2001

Abstract

The main purpose of this study is focused on the feasibility, reliability, and applicability of detecting the rebar (reinforcing steel bar) corrosion in concrete blocks by using impact-echo method associated with three electrochemical methods; that is open-circuit potential (OCP), direct current (DC) polarization, and alternating current (AC) impedance. The result of present study indicates that the impact-echo method can certainly detect the development of microcrack in the concrete blocks. With respect to predicting corrosion damage, the displacement spectrum obtained from the impact-echo method should be transferred as acceleration spectrum. Thus, the degree of corrosion damage can be predicted from relative amplitude obtained from acceleration spectrum. The OCP method can evaluate the corrosion state of steel in concrete. However, it is not useful in predicting the corrosion damage of the interior of the specimen. Both the DC polarization and AC impedance methods can predict the corrosion rate. The corrosion thickness of specimen obtained from integrating the corrosion rate can directly evaluate corrosion damage. It is very obvious that the proposed method can be applied to the nondestructive testing for reinforced concrete (RC) structures.

Keywords: Acceleration; Vibration; Corrosion; Electrochemical method; Concrete

1. Introduction

The corrosion damage of reinforced concrete (RC) structures is often a severe and invisible injury. At the present, evaluating the corrosion state is done by measuring both the corrosion potential and corrosion rate of steel in concrete using electrochemical method. However, the electrochemical method cannot indicate the failure state of RC structures. As to nondestructive testing widely used in civil engineering, both the physical properties and internal and external crack state of RC structures are the major tests done. The results obtained from the method of nondestructive testing can only provide qualitative description for RC structures. Thus, the results of nondestructive testing cannot predict the bearing capacity and service life of RC structures. Thus, if one uses the measurement results of impact-echo method associated with electrochemical method, then one takes into account every aspect of corrosion damage evaluation.

Carino et al. [1] established the impact-echo method wherein the transient time domain waveforms obtained from the impact of a steel sphere on a concrete slab containing artificial flaws are recorded and analyzed in the frequency domain. Carino and Sansalone [2] provided a brief explanation of the impact-echo method and presented results that illustrate the capabilities of the method to locate a variety of flaws in plain and reinforced concrete. Sansalone and Carino [3] carried out experiments on laboratory specimens that contained artificial flaws at known locations. Frequency analysis of recorded surface displacement waveforms was used to determine the location of honeycombing, the depth of surface-opening cracks, and ungrouted ducts. Sansalone and Carino [4] used the impact-echo method to detect determination in RC slabs with and without asphalt concrete overlays. Lin et al. [5] studied experimentally the integrity of concrete shafts and piles containing flaws and embedded in soil using the impact techniques. Sansalone et al. [6] summarized the developments in the impact-echo technique for

* Corresponding author. Tel.: +886-2-224-622-192; fax: +886-2-246-323-75.

E-mail address: mliang@mail.ntou.edu.tw (M.-T. Liang).

0008-8846/01/$ – see front matter
PII: S0008-8846(01)00569-5

locating defects in concrete structures. Pratt and Sansalone [7] used artificial intelligence called neural network to automate impact-echo signal interpretation from concrete slabs contained voids and cracks. Lin and Sansalone [8] demonstrated the feasibility of using the impact-echo method for detecting flaws in RC beams and columns. Lin and Sansalone [9,10] studied the transient response of thick circular, square, and rectangular bars subjected to transverse elastic point impact. Cheng and Sansalone [11] used finite element method and impact-echo method to demonstrate the effects of different variables with rebar diameter, rebar depth, impact duration, and impact-echo test configuration. Cheng and Sansalone [12] used the impact-echo method for detecting delaminations in concrete plate-like structures such as bridge decks, slabs, and walls. Lin and Sansalone [13] determined the transient elastic impact response of thick-walled hollow cylindrical structures and determined how this response was effected by the presence of flaws in the cylinder. Lin and Sansalone [14,15] demonstrated that the impact-echo method can be used for integrity testing for concrete pipes, mine shaft liners, and tunnel liners in contact with soil and rock. Sakata and Ohtsu [16] used ultrasonic spectroscopy to measure the depth of surface cracks in concrete members. Lin and Sansalone [17] demonstrated how the unbounded fraction at an interface affects impact-echo response. Lin et al. [18] explained how bond tensile strength affects impact-echo response. Jaeger et al. [19] used the impact-echo method to detect both complete and partial voids in grouted tendon ducts of post-tensioned concrete structures. Lin and Su [20] determined the depth of surface-opening cracks in concrete structures with the use of stress waves so that a safety evaluation of such cracked structures can be subsequently performed. Sansalone [21] provided, for the first time, a unified explanation of the impact-echo method as it applies to the testing of structural concrete elements. Sansalone et al. [22] described the time-of-flight technique that can be used in conjunction with techniques for measuring P wave speed to determine the depth of surface-opening cracks in concrete structures. Lin et al. [23] provided a clear explanation for the effects caused by rebars on transient stress wave propagation and crack depth measurement. Lin et al. [24] demonstrated the capability of the time-of-flight diffraction technique for measuring the depth of surface-opening cracks in RC structures and determining errors in measurement. Hill et al. [25] described an investigation of the use of the impact-echo method and the excitation of cross-sectional modes to distinguish between a grouted and an ungrouted duct in a rectangular beam. Yeih and Huang [26] used the amplitude attenuation method in ultrasonic testing to evaluate the corrosion damage of RC members. To date, however, no studies have attempted to study the corrosion damage of rebar in concrete using the impact-echo method associated with the electrochemical method. This is a notable shortcoming, because the use of the impact-echo method in previous studies may have resulted in detection of flaws in concrete structures.

The main purpose of this paper is to study the feasibility, reliability, and applicability of the rebar corrosion in concrete blocks using impact-echo method associated with electrochemical methods. The result of this study may give aid for applying the impact-echo technique in predicting the rebar corrosion in concrete.

Table 1
The chemical composition of steel rebars

Element	C	Cu	Si	Mn	P	S	Ni	Cr	Mo	Sn	Fe
Weight percent	0.36	0.23	0.20	0.61	0.04	0.03	0.11	0.12	0.01	0.02	balance[a]

[a] Balance means valenced.

Table 2
The concrete mix designs

Label	Water/cement ratio	Mix proportion (kg/m^3)				
		Water	Cement	Sand	Aggregate	SP[a]
Set A	0.35	213.5	610.2	494	1010.8	6.1
Set B	0.4	213.5	533.9	565.4	1010.8	5.34

[a] SP is an F-type superplasticizer.

2. Theoretical background

The technique of the impact-echo method [1] involves introducing a transient stress pulse into the test object by mechanical impact and monitoring the surface displacements caused by the arrival of reflections of the pulse from internal defects and external boundaries. Recorded displacement waveforms are analyzed in the frequency domain. If the velocity of the wave is known, the distance to a defect or an interface can be calculated by measuring the round-trip travel time from the start of the wave to the reception of the echo. Let C_P be P wave velocity in concrete plate and T the thickness from bottom or internal defects to

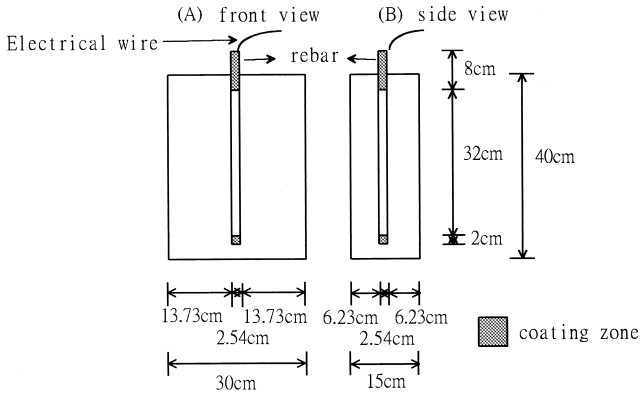

Fig. 1. Specimen size and rebar position of Set A.

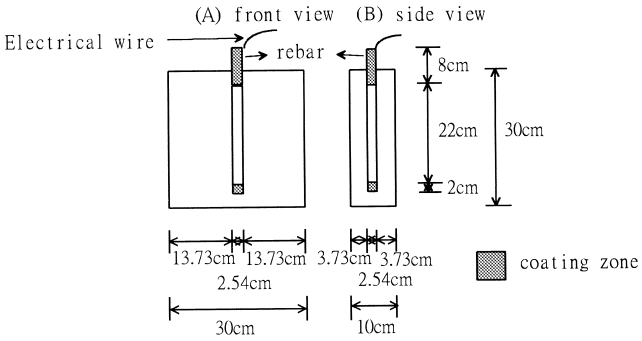

Fig. 2. Specimen size and rebar position of Set B.

surface. The travel time, Δt, between the successive arrivals of P wave echoes from the bottom surface of the plate is given in Eq. (1):

$$\Delta t = \frac{2T}{C_P}. \tag{1}$$

The corresponding frequency, f, of echo arrivals is

$$f = \frac{1}{\Delta t} = \frac{C_P}{2T}. \tag{2}$$

When the underlying material is acoustically stiffer (has a larger acoustic impedance), such as at a concrete–steel interface, the amount of reflection is also determined by the difference between the acoustic impedance of two materials. In this case, Eq. (2) is no longer valid. The equation relating the measured frequency of reflections from acoustic stiffer interface f_s to the depth of this interface T_s is

$$f_s = \frac{C_P}{4T_s}. \tag{3}$$

Cheng and Sansalone [11] found that the steel diameter (D) and embedded depth (T_s) are affected the results of spectral analysis. When the value of D/T_s is less than 0.3, the peak value from steel reflection in spectrum will disappear or decrease. In this case, it is very difficult to analyze the

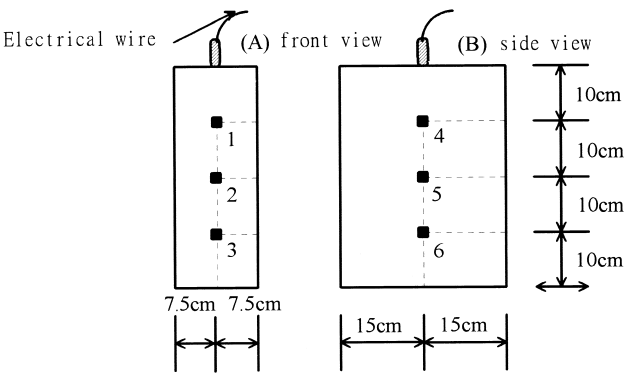

The impact source is just above 5cm on the mark number.
The received point is from 1 to 6.

Fig. 3. The impact position of Set A.

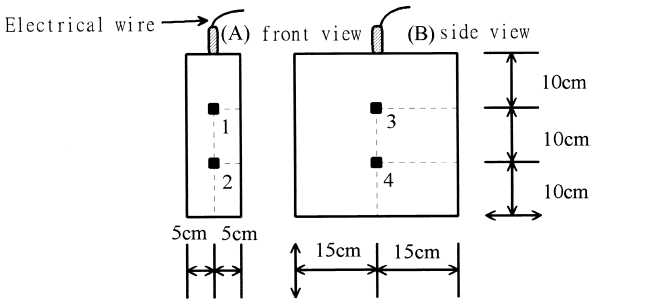

The 1-4 impact source is just above 5cm on the mark number.
The recived point is from 1 to 4.

Fig. 4. The impact position of Set B.

depth of steel. Thus, Eq. (3) should be modified by multiplying by a factor ξ as follows (Eq. (4)):

$$f_s = \frac{\xi C_P}{4T_s} \tag{4}$$

where ξ is defined by the following empirical relationship (Eq. (5)):

$$\xi = -0.6\frac{D}{T_s} + 1.5, \quad 0.3 \le \frac{D}{T_s} \le 1. \tag{5}$$

These formulas mentioned above are only used to detect flaw in the plates. If these formulas are applied to predict the flaw in the beams and columns, then the frequency spectrum analysis becomes very difficult. This phenomenon can be proven by Lin and Sansalone [8] who showed that the transient impact response of a solid beam of column is composed of a number of resonant frequencies caused by cross-sectional modes of vibration. These modes depend on the geometry and dimensions of a beam or column's cross-section. They also showed that the presence of a defect disrupts the frequency pattern produced by the cross-sectional modes.

For either the direct current (DC) linear polarization method or the alternating current (AC) impedance method, the polarization resistance, $R_p = \Delta E/\Delta i$ ($\Omega \cdot cm^2$), where ΔE (V) is the potential difference and Δi (A/cm^2) is the current

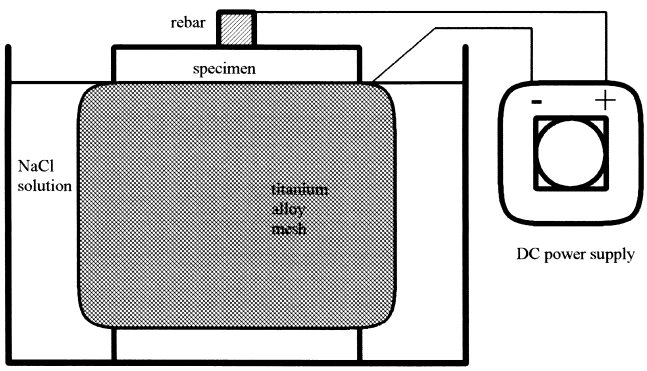

Fig. 5. Scheme of accelerated corrosion.

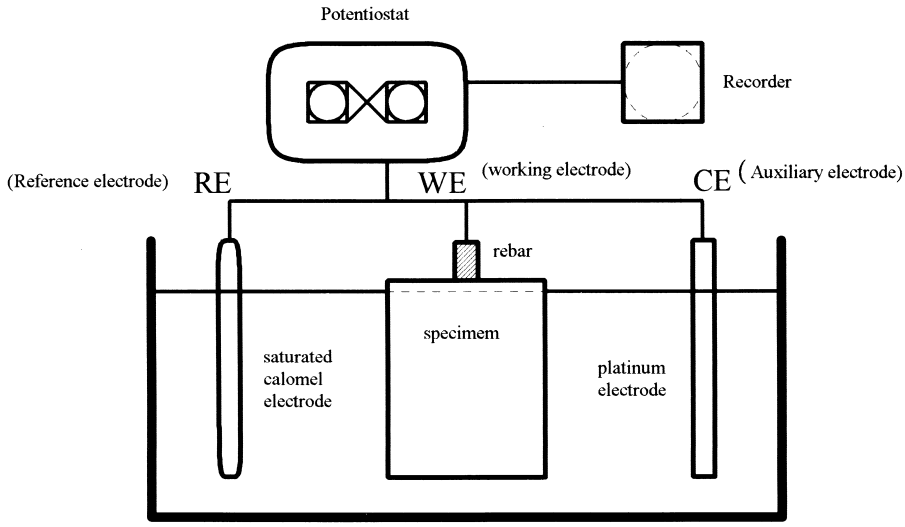

Fig. 6. Experimental scheme of DC polarization (OCP).

density difference, can be measured. The corrosion current density, i_{corr} (A/cm^2), can be represented as

$$i_{corr} = \left[\frac{\beta_a\beta_b}{2.303(\beta_a+\beta_b)}\right]\times\frac{\Delta i}{\Delta E} = B\times\frac{1}{R_p} \quad (6)$$

where β_a and β_b represent the Tafel's slopes of the anodic polarization curve and the cathodic polarization curve, respectively. The value of B is often taken as 26 mV [27] for steels in an alkaline environment (the pH value for a concrete environment is above 12.8), Eq. (6) is called the Stern–Greary equation [28].

After the corrosion current density is obtained, the instantaneous corrosion rate, Γ_{corr}, can be calculated from Faraday's law as (Eq. (7))

$$\Gamma_{corr} = \frac{i_{corr}}{nF}\times\frac{W_{Fe}}{D_{Fe}} \quad (7)$$

where Γ_{corr} (cm/s) represents the thickness loss of the steel per unit of time, corrosion engineers often choose mils per year (mil/year) or micrometer per year (μm/year) as the unit of Γ_{corr}, F is the Faraday's constant, which is 96,500 C/mol, W_{Fe} (55.8 g/mol) is the atomic weight of the iron, D_{Fe} (7.86 g/cm^2) is the density of the iron, and n is the valence of oxidant for the following oxidation reaction (Eq. (8))

$$Fe\rightarrow Fe^{2+} + 2e^{-}. \quad (8)$$

Thus, n is equal to 2.

The thickness loss can be obtained by integrating the area of the instantaneous corrosion rate versus the time curve, which means that the thickness loss, s, is expressed as (Eq. (9))

$$s(t) = \int_0^t \Gamma_{corr}(t)\mathrm{d}t. \quad (9)$$

From the definition of the instantaneous corrosion rate, it is easy to find that the loss of thickness in a function of time and that it represents the average thickness loss of iron at a specific time.

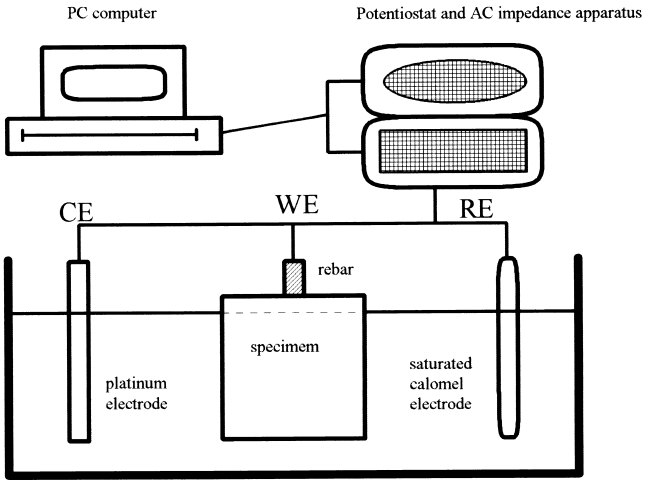

Fig. 7. Experimental scheme of AC impedance.

3. Experimental method

The rebar used in this research was made of medium carbon steel, the chemical composition of which is listed in Table 1. One size of rebars (#8 rebar with diameter 25.4 mm) was used. Two concrete mixes were selected as shown in Table 2. The size of RC blocks divides into Sets A and B and the rebar was embedded in the concrete as shown in Figs. 1 and 2. Part of the surface of the rebar was coated with epoxy. The size of Set A is $40\times30\times15$ cm^3, whereas the size of Set B is $30\times30\times10$ cm^3. The water/cement ratios of 0.35 and 0.4 were adopted and represented as I and II, respectively. Electrical wires were connected to the rebars to speed up the corrosion damage and electrochemical

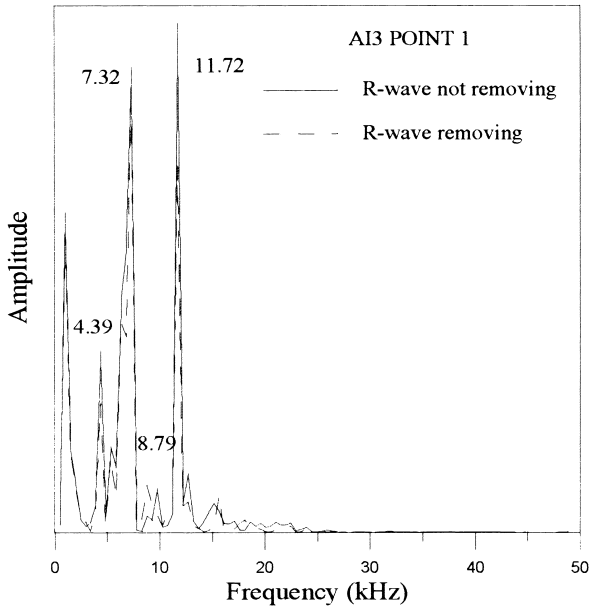

Fig. 8. Initial displacement spectrum of the first point in the AI3 specimen.

measurements. The specimens were labeled AI1, AI2, AI3, AII1, AII2, AII3, BI1, BI2, BI3, BII1, BII2, and BII3, where the letters represented the Sets A and B, the roman numerals represented the water/cement ratios 0.35 and 0.4, and the numbers represented the number of RC concretes. For each set, three specimens were prepared to check the consistency of the data. After demolding, the specimens were cured using the standard curing method for 28 days.

To perform impact-echo testing, one first marks the position of impact source and receiver on the RC blocks as shown in Figs. 3 and 4. The specimens were immersed in 3.5% NaCl solution and connected to a DC power supply to accelerate the corrosion process as shown in Fig. 5. The rebar was arranged as an anode and titanium alloy mesh as a cathode. The constant current density, 1 mA/cm^2, was impressed according to previous studies [20]. Once every 24 h, the impressed current was cut off, and open-circuit potential (OCP) (Fig. 6) values, DC polarization (Fig. 6) resistance values, and AC impedance (Fig. 7) values were sequentially measured for each specimen 1 h after current cut-off. After the electrochemical measurements were made, the specimens were removed from the tanks, and impact-echo testing was conducted.

The experimental procedures are described in detail as follows:

(a) Mark impact test number on the surface of RC blocks and then put it into water until saturation.

(b) Measure in turn the corrosion state by using OCP, DC polarization, and AC impedance methods. There should be a short period of rest when measuring the RC blocks using both DC polarization and AC impedance methods in order to avoid interference.

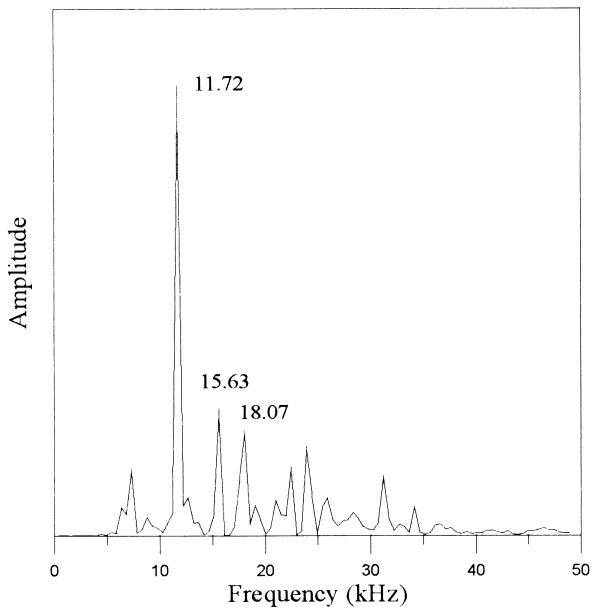

Fig. 9. Initial acceleration spectrum of the first point in the AI3 specimen.

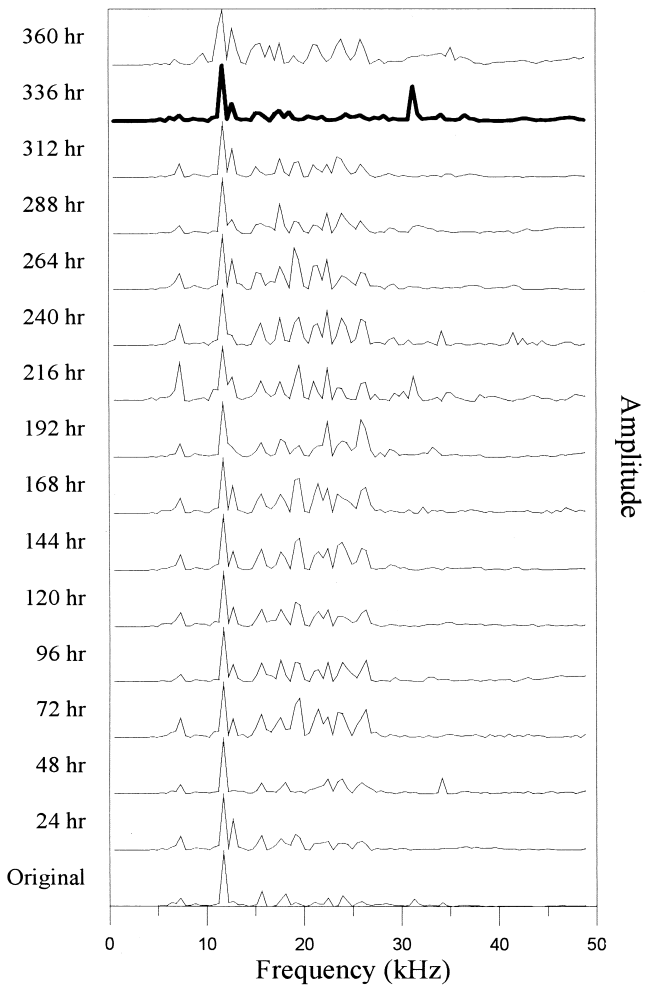

Fig. 10. Acceleration spectrum of the first point in the AI3 specimen.

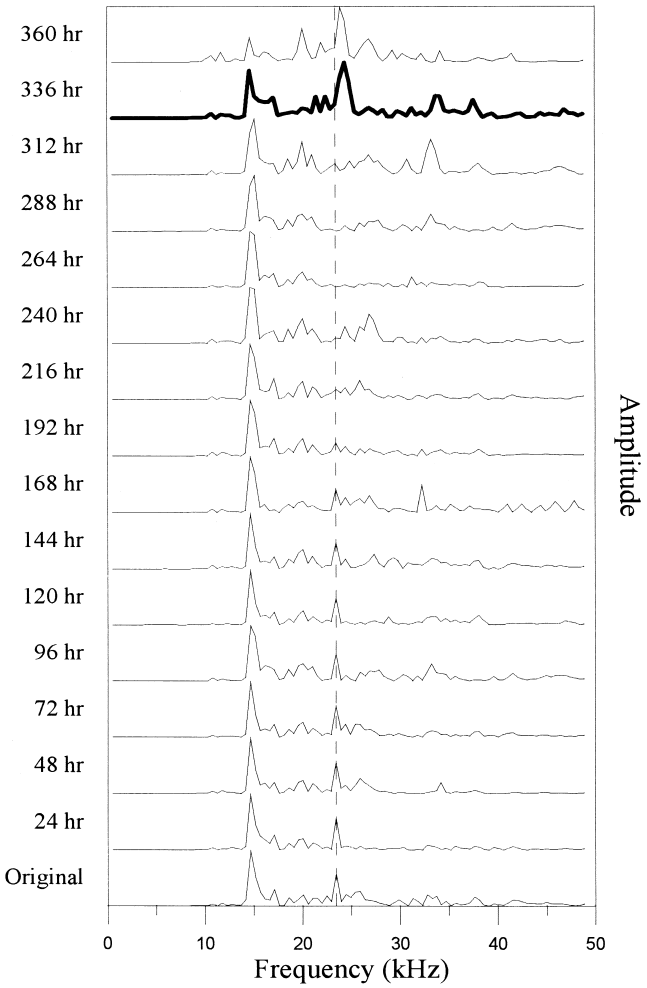

Fig. 11. Acceleration spectrum of the fourth point in the AI3 specimen.

(c) After measuring using the electrochemical method mentioned earlier, take out the RC blocks from the water tank and then expose to air. Execute the impact-echo test when the RC blocks have dried.

(d) Put the RC block into the sodium chloride solution and wrap it with barbed-wire entanglements (titanium alloy mesh). Connect the DC for increasing rebar corrosion.

(e) Turn off the source of electricity after increasing corrosion for 24 h. The RC blocks were left untreated for an hour until ion equilibrium is attained in the specimen. Execute the measurements repeatedly according to the (b), (c), (d), and (e) processes until the specimen fractures.

After impact test and received data, one gets a frequency spectrum from personal computer by the fast Fourier transform and then carries out the analysis.

4. Results and discussion

The P wave velocity, C_P, in RC blocks with water/cement ratio of 0.35 is 4600 m/s. Fig. 8 shows the initial displacement spectrum of the first point in AI3 specimen. It is indicated in Fig. 8 that the displacement spectrum was guided by cross-sectional mode. Most of the energy due to impact are concentrated on the cross-sectional mode. It is also found that when the R wave was removed, most of the peak positions in the displacement spectrum are not changed while the energy distribution is changed. This means that when the R wave was removed, most of the reflections of P wave were received in the displacement waves. These reflections of P wave can promote the energy with high frequency. Fig. 9 indicates the initial acceleration spectrum of the first point in AI3 specimen. It is found from Fig. 9 that the amplitude value of high frequency is very obviously promoted. With respect to detecting cracks, the cracks have to develop enough to interfere with the cross-sectional mode. The microcracks due to corrosion cannot interfere with the basic cross-sectional mode while it can reduce the cross-sectional mode of high frequency. Thus, the acceleration spectrum aids in finding early the growth of microcracks due to corrosion. Fig. 10 shows the acceleration spectrum of the first point of AI3. The frequency value corresponding to rebar position is 23.26 kHz for AI3 specimens. It is found that the peak value of 11.72 kHz during increasing corrosion is unchanged until the specimen cracks after 336 h. At this time, the peak value of frequency

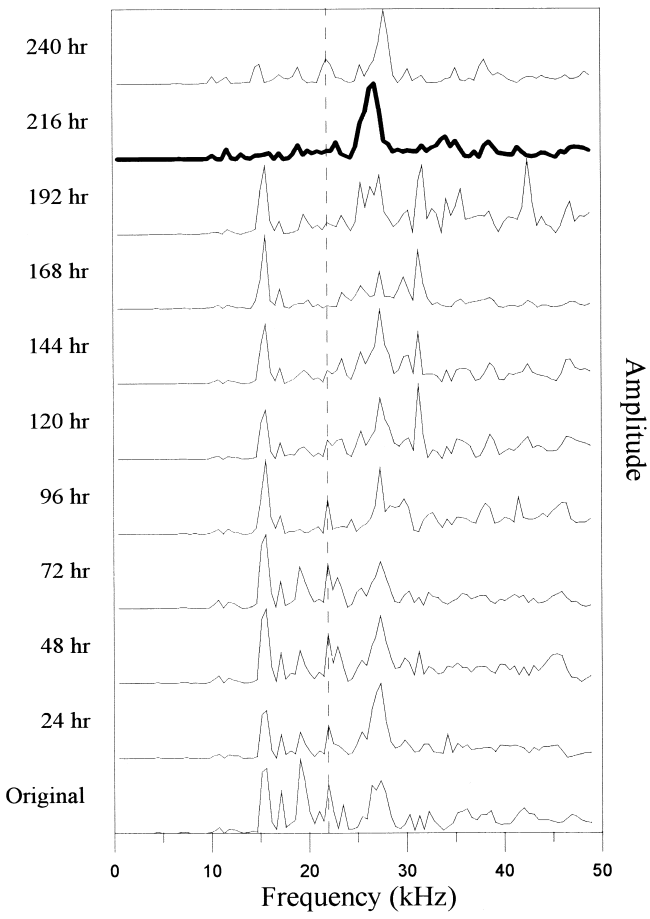

Fig. 12. Acceleration spectrum of the fifth point in the AII3 specimen.

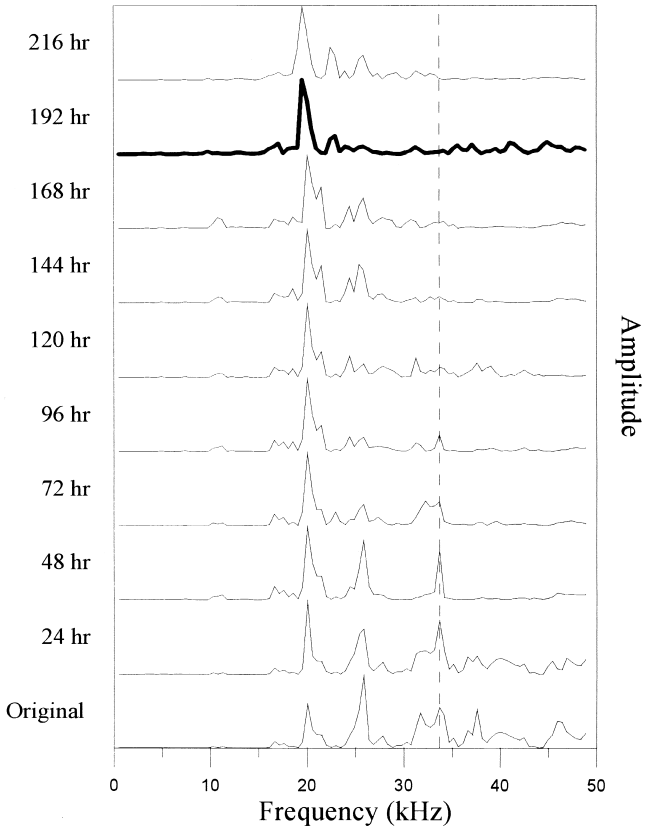

Fig. 13. Acceleration spectrum of the third point in the BI3 specimen.

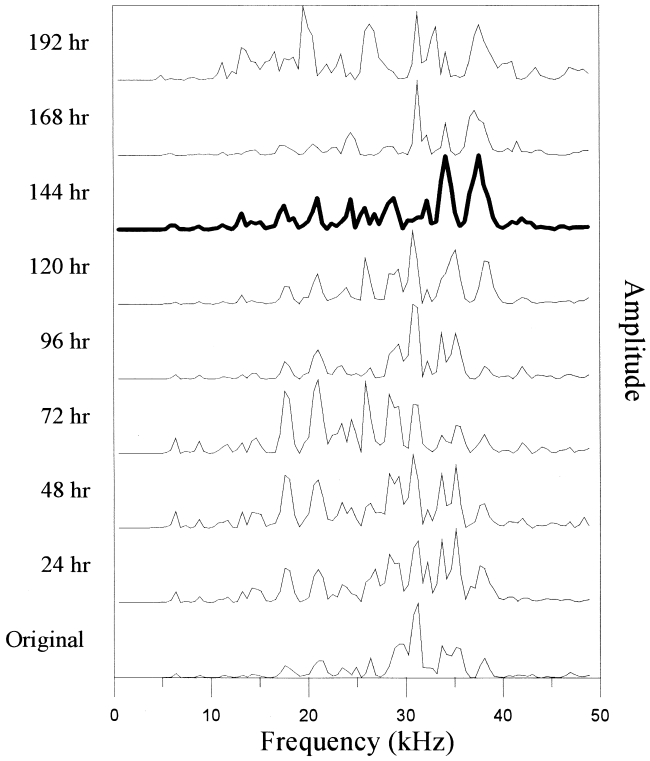

Fig. 14. Acceleration spectrum of the second point in the BII3 specimen.

of this specimen is decreasing. This frequency corresponds to the mode of the basic cross-section. The peak values of 15.63 and 18.07 kHz represent two modes of cross-section. They are not changed during the initial stage whereas they are decreasing after 246 h. The reason for these variations results from the different energy of impact source and partly the influence of microcrack due to corrosion. After 72 h, one can see many peak values between 15 and 25 kHz. They correspond to the depth of crack ranging from 9 to 15 cm. These are located just above the rebar circumference. This proves that there are some microcracks in the specimen after 72 h. This also shows that the impact-echo method can certainly detect the development of microcrack in the specimen according to these analytical processes. Fig. 11 indicates the acceleration spectrum of the fourth point of AI3. One cannot find the peak value of 23.26 kHz from the acceleration spectrum around 240 h. This is partly because the specimen density decreases due to rust occurrence. The impedance is also decreased. Thus, the amplitude of the reflection wave declines. The other reason is that the microcrack around rebar increases the scatter effect to the incident wave. This occurs in the lower energy of reflective wave. It is observed from the specimen surface that the impact position of the fourth point is vertical to the crack. Hence, it cannot determine the crack location. The P wave velocity, C_P, in RC blocks with water/cement ratio 0.4 is 4100 m/s. Fig. 12 denotes the acceleration spectrum of the fifth point of AII3. The major analytical frequencies are 15.14, 19.04, and 27.34 kHz. The frequency corresponding

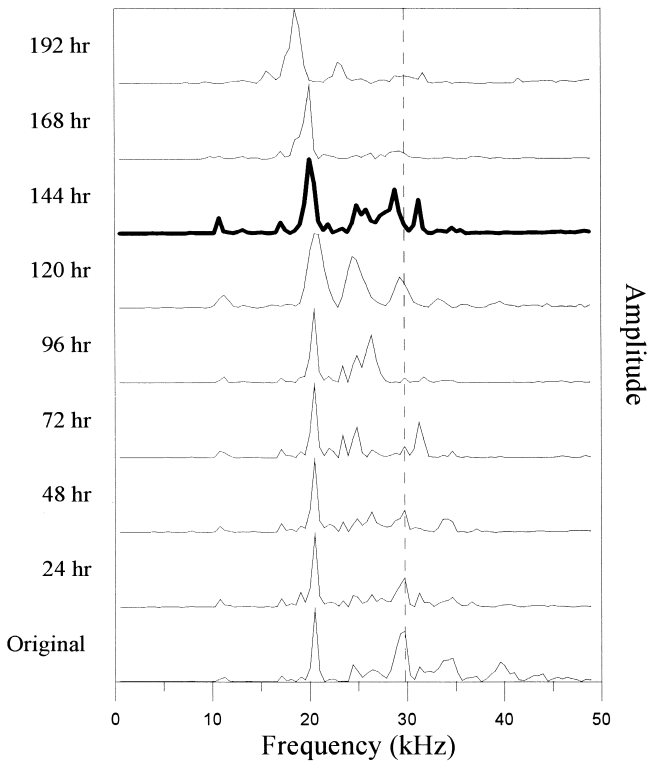

Fig. 15. Acceleration spectrum of the third point in the BII3 specimen.

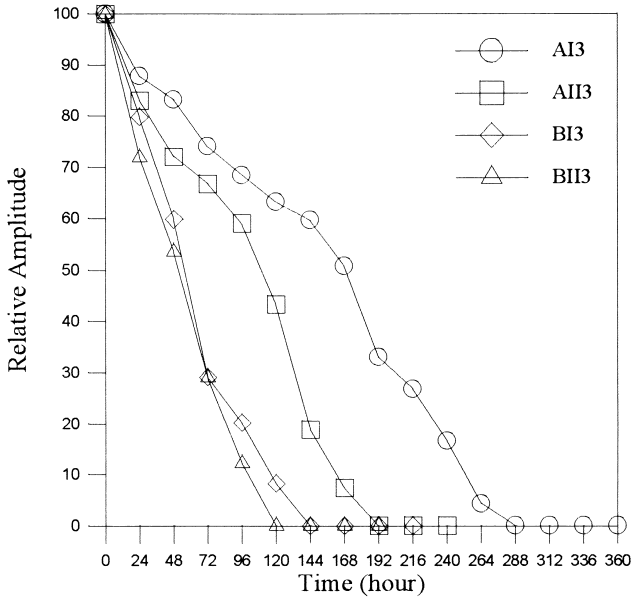

Fig. 16. Relationship between relative amplitude and time.

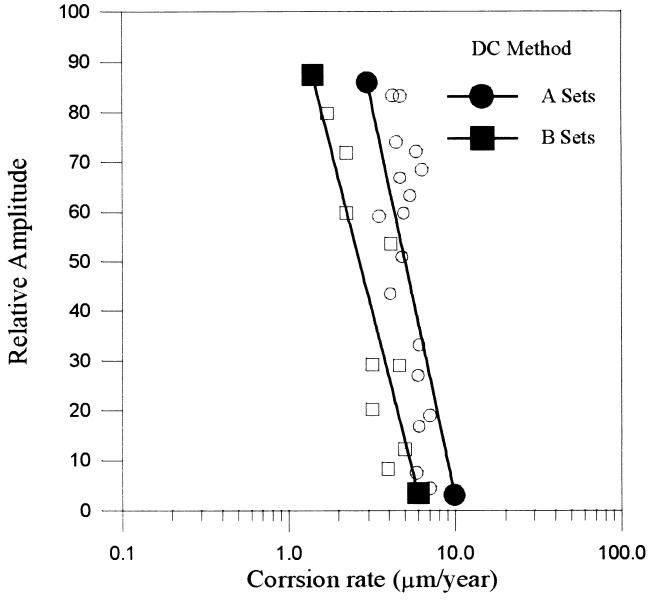

Fig. 18. Relationship between relative amplitude and corrosion rate.

to rebar position is 21.97 kHz. This peak disappeared after 168 h. Relying on this phenomenon, it provides a warning before the specimen noncracked.

Fig. 13 shows that the acceleration spectrum of the third point of BI3. The major analysis emphasizes the peak values 20.02 and 25.88 kHz, and the 33.69 kHz that corresponds to rebar position. At about 144 h, the 25.88-kHz frequency presented that the cross-sectional mode has been changed and the peak of 33.69 kHz has disappeared. Since the energy of each impact is closed, the peak value observed from spectrum gradually declined and this means that the rebar corrosion is very serious. Fig. 14 indicates the acceleration spectrum of the second point of BII3. The surface of specimen cracks at about 144 h. After 96 h, the frequency in Fig. 14 has an obvious variation. It is worth to point out that the crack depth corresponding to the major peak value ranged from 5 to 7 cm before the specimen split. Fig. 15 denotes the acceleration spectrum of the third point of BII3. The peak value of 29.7 kHz corresponding to rebar disappeared before the crack occurrence of specimen. This peak value gradually decreased before 96 h. Since the energy of each impact source is different, the high and low peak values do not directly detect the degree of rebar corrosion. Hence, if one wishes to combine the results

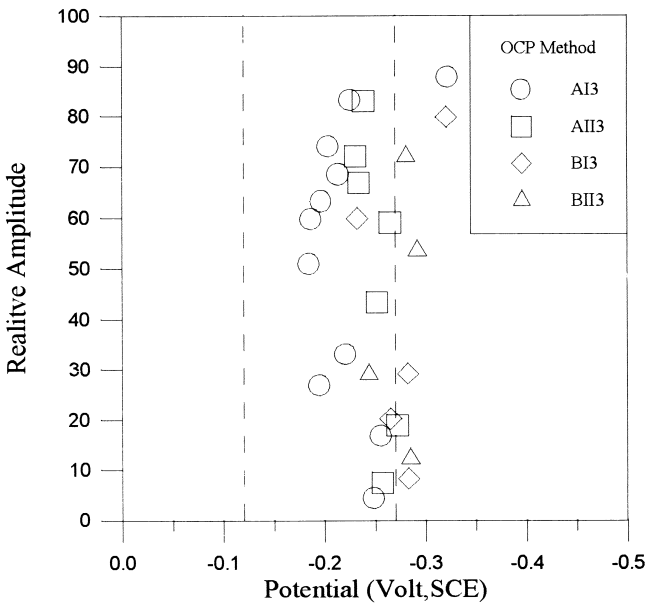

Fig. 17. Relationship between relative amplitude and OCP.

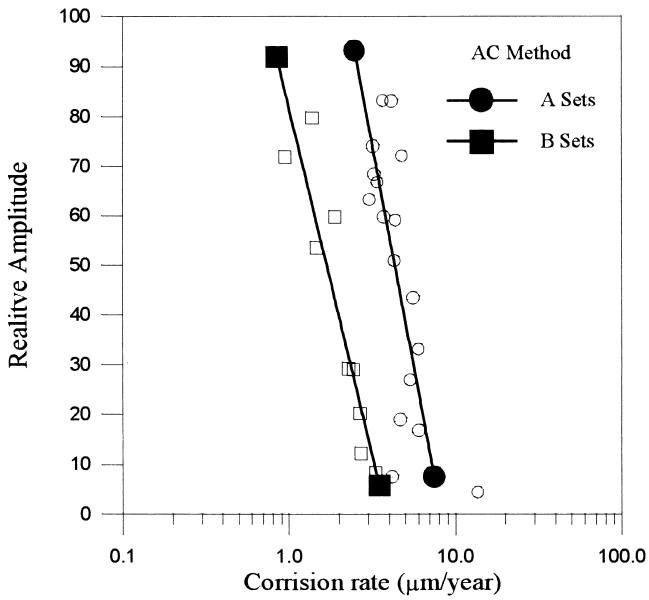

Fig. 19. Relationship between relative amplitude and corrosion rate.

Table 3
Regression formulas between relative amplitude and corrosion rate

Method	Number	Regression formulas	Relative coefficient, R
DC method	A	$y=-158.46 \log x+161.38$	0.9423
	B	$y=-132.88 \log x+106.94$	0.9625
AC method	A	$y=-78.09 \log x+164.7$	0.9546
	B	$y=-60.86 \log x+82.07$	0.9713

obtained from impact-echo method with those results obtained from the electrochemistry method, then one needs to use another analytical stage.

Fig. 16 shows the relationship of amplitude versus the time of accelerated rebar corrosion. It is found that BII3 has a deteriorated degree of relative amplitude in the first measurement. The other specimens are BI3, AII3, and AI3. In addition, in BII3, the first specimen deteriorated to zero. This certainly results from the cover thickness and the highest water/cement ratio. Because BII3 has the lowest cover thickness and water/cement ratio, the corrosion degree of BII3 is severely deteriorated under the same time. Comparing both Sets A and B of specimens, Set B is confirmedly more deteriorated under the same time than the Set A. It is to be understood that the cover thickness is the important parameter of control corrosion in this experimental study. Thus, using the relative amplitude to evaluate the corrosion damage is confirmedly serviceable. Fig. 17 expresses the relative amplitude versus the potential of OCP. The data of each specimen are varied and are not related to one another. However, most of data are allocated between -0.12 and -0.27 V SCE (saturated calomel electrodes). Based on ASTM C876-91 [29], the corrosion rate ranged from 10% to 90%. According to the variation of relative amplitude, the measured results obtained from the OCP method indicate that it has difficulties in predicting the corrosion state. However, there are many microcracks in the specimens subjected to corrosion damage. Thus, the corrosion damage of structure is related to the progress probability of the transient response of rebar corrosion. The OCP method just provides a reference. The OCP method is not useful in predicting the corrosion damage of the interior of specimen.

Figs. 18 and 19 express the relationship of the relative amplitude versus the corrosion rate of DC and AC, respectively. Their regression formulas are also shown in Table 3.

Table 4
Linear regression formulas between relative amplitude and corrosion thickness

Method	Number	Linear regression formulas	Relative coefficient, R
DC method	AI3	$y=-554.35x+96.14$	0.9603
	AII3	$y=-943.24x+98.85$	0.9624
	BI3	$y=-2287.2x+79.26$	0.9805
	BII3	$y=-1776.69x+77.24$	0.9883
AC method	AI3	$y=-678.96x+90.15$	0.9746
	AII3	$y=-1035.75x+93.74$	0.9603
	BI3	$y=-2848.1x+77.63$	0.9825
	BII3	$y=-3771.69x+72.83$	0.9889

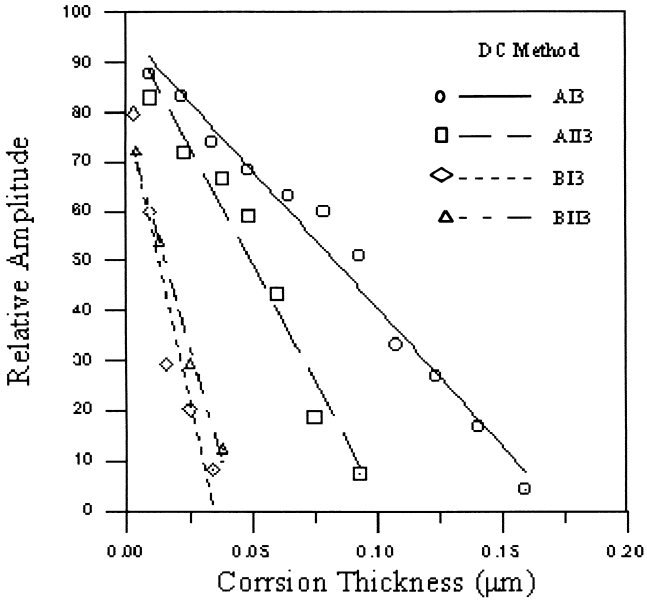

Fig. 20. Relationship between relative amplitude and corrosion thickness.

One can find the best fitting curve on the regression analysis. It is observed on the same specimen that the slope obtained from DC method is twice that of the AC method. This means that under the same degree of corrosion damage, the corrosion rate measured by the DC method is larger than that measured by the AC method. In other words, if both the DC and AC methods are used to select two specimens, and same corrosion rates were obtained, then the corrosion damage of specimen detected by the AC method is more severe.

The corrosion thickness is obtained from the integral of corrosion rate with respect to time. This is the accumulated result of rust larger inward intruding the rebar before measurement. Table 4 indicates the linear regression

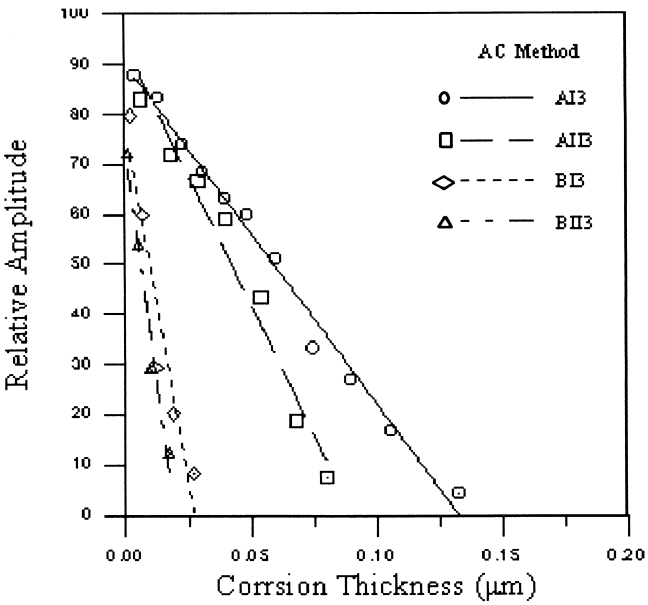

Fig. 21. Relationship between relative amplitude and corrosion thickness.

formulas between corrosion thickness and relative amplitude for the DC and AC methods. It is found in Table 4 that in the case of the truncated distance of each regression formula versus *y*-axis, the corrosion thickness is negative value instead of zero when the relative amplitude is 100. However, it is impossible for the corrosion thickness to have a zero value. This means that the rebar in specimen has corrosion at initial measurement. From this phenomenon, one has to discuss each specimen and modify the regression formulas. One keeps the slope invariable in order to set corrosion thickness with a zero value whereas the relative amplitude with 100 values. If one substitutes the originally truncated distance of *y*-axis into *y* value then the value of *x*-axis can be considered the corrosion thickness before measuring. Figs. 20 and 21 denote the relationship between relative amplitude and corrosion thickness for DC and AC methods, respectively. Every result is obviously different and tends to linearly decrease. One can use this method in practical applications. For instance, carry out the measurement of impact-echo and corrosion rate at a transient time to any RC structure. Transform the corrosion rate with respect to time to corrosion thickness. The linear regression formula is obtained from the relationship between relative amplitude and corrosion thickness. One can calculate the corrosion thickness in the past and at present, respectively. This is very useful for predicting corrosion damage.

5. Conclusions

This research uses the impact-echo method combined with three electrochemical methods to detect the rebar corrosion in concrete, that is, OCP, DC polarization, and AC impedance. The impact-echo method is certainly able to detect the development of microcrack in the RC blocks. The OCP method is not useful in predicting the corrosion damage of the interior of specimen. Both DC polarization and AC impedance methods can predict the corrosion rate and corrosion thickness of specimen.

This paper has provided another method for evaluating rebar corrosion damage in concrete by the impact-echo method. Although the proposed method is not as mature as traditional electrochemical methods, it appears that this proposed method is a fruitful area for further research.

References

[1] J.N. Carino, M. Sansalone, N.N. Hsu, Flaw detection in concrete by frequency spectrum analysis of impact-echo waveforms, vol. 12, Int. Adv. Nondestr. Test., Gordon & Breach Science, 1986, pp. 117–146.
[2] N.J. Carino, M. Sansalone, Impact-echo: A new method for inspecting construction materials, Proc. Conf. NDT&E Manuf. Constr., University of Illinois at Urbana-Champaign, 1988.
[3] M. Sansalone, N.J. Carino, Impact-echo method, Concr. Int. 10 (4) (1988) 38–46.
[4] M. Sansalone, N.J. Carino, Detecting delaminations in concrete slabs with and without overlays using the impact-echo method, ACI Mater. J. 86 (2) (1989) 175–184.
[5] Y. Lin, M. Sansalone, N.J. Carino, Impact-echo response of concrete shafts, Geotech. Test. J., ASTM 14 (2) (1991) 121–137.
[6] M. Sansalone, Y. Lin, D. Pratt, C.C. Cheng, Advancements and new applications in impact-echo testing, Concr. Struct., (1992) 135–150.
[7] D. Pratt, M. Sansalone, Impact-echo signal interpretation using artificial intelligence, ACI Mater. J. 89 (2) (1992) 178–187.
[8] Y. Lin, M. Sansalone, Detecting flaws in concrete beams and columns using the impact-echo method, ACI Mater. J. 89 (4) (1992) 394–405.
[9] Y. Lin, M. Sansalone, Transient response of thick circular and square bars subjected to transverse elastic impact, J. Acoust. Soc. Am. 91 (2) (1992) 885–893.
[10] Y. Lin, M. Sansalone, Transient response of thick rectangular bars subjected to transverse elastic impact, J. Acoust. Soc. Am. 91 (5) (1992) 2674–2685.
[11] C.C. Cheng, M. Sansalone, Effect on impact-echo signals caused by steel reinforcing bars and voids around bars, ACI Mater. J. 90 (5) (1993) 421–434.
[12] C. Cheng, M. Sansalone, The impact-echo response of concrete plate containing delaminations: Numerical, experimental and field studies, Mater. Struct. 26 (1993) 274–285.
[13] J.M. Lin, M. Sansalone, The transverse elastic impact response of thick hollow cylinders, J. Nondestr. Eval. 12 (2) (1993) 139–149.
[14] J.M. Lin, M. Sansalone, Impact-echo response of hollow cylindrical concrete structures surrounded by soil and rock: Part I. Numerical studies, Geotech. Test. J., ASTM 17 (2) (1994) 207–219.
[15] J.M. Lin, M. Sansalone, Impact-echo response of hollow cylindrical concrete structures surrounded by soil and rock: Part II. Experimental studies, Geotech. Test. J., ASTM 17 (2) (1994) 220–226.
[16] Y. Sakata, M. Ohtsu, Crack evaluation in concrete members based on ultrasonic spectroscopy, ACI Mater. J. 92 (6) (1995) 686–698.
[17] J.M. Lin, M. Sansalone, Impact-echo studies of interfacial bond quality in concrete: Part I. Effects of unbounded fraction of area, ACI Mater. J. 93 (3) (1996) 223–232.
[18] J.M. Lin, M. Sansalone, R. Poston, Impact-echo studies of interfacial bond quality in concrete: Part II. Effects of bond tensile strength, ACI Mater. J. 93 (4) (1996) 318–326.
[19] B.J. Jaeger, M.J. Sansalone, R.W. Poston, Detecting voids in grouted tendon ducts of post-tensioned concrete structures using the impact-echo method, ACI Mater. J. 93 (4) (1996) 462–473.
[20] Y. Lin, W.C. Su, Use of stress waves for determining the depth of surface-opening cracks in concrete structures, ACI Mater. J. 93 (5) (1996) 494–505.
[21] M. Sansalone, Impact-echo: The complete story, ACI Struct. J. 94 (6) (1997) 777–786.
[22] M. Sansalone, J.M. Lin, W.B. Streett, Determining the depth of surface-opening cracks using impact-generated stress wave and time-of-flight techniques, ACI Mater. J. 95 (2) (1998) 168–177.
[23] Y. Lin, T. Liou, C. Hsiao, Influence of reinforcing bars on crack depth measurement by stress wave, ACI Mater. J. 95 (4) (1998) 407–418.
[24] Y. Lin, T. Liou, W.H. Tsai, Determining crack depth and measurement errors using time-of-flight diffraction techniques, ACI Mater. J. 96 (2) (1999) 190–195.
[25] M. Hill, J. McHugh, J.D. Turner, Cross-sectional modes in impact-echo testing of concrete structures, J. Struct. Eng. 126 (2) (2000) 228–234.
[26] W. Yeih, R. Huang, Detection of the corrosion damage in reinforced concrete members by ultrasonic testing, Cem. Concr. Res. 28 (7) (1998) 1071–1083.
[27] R.K. Dhir, M.R. Jones, M.J. Macarthy, Quantifying chloride-induced corrosion from half-cell potential, Cem. Concr. Res. 23 (1993) 1443–1454.
[28] C. Andrade, Monitoring techniques, in: P. Schiessl (Ed.), Corrosion of Steel in Concrete, Chapman & Hall, London, 1988, pp. 79–95.
[29] ASTM C876-91, Standard Test Method for Half-Cell Potentials of Uncoated Reinforcing Steel in Concrete, ASTM, Philadelphia, 1991.